Differential Roles of the Salience Network During Prediction Error Encoding and Facial Emotion Processing Among Female Adolescent Assault Victims

Supplemental Information

Reinforcement Learning Tasks

Participants completed a three-arm bandit task using either social or neutral stimuli (Supplemental Figure S1). During the social task, participants were directed to select among three mock people in which to invest $10, and the mock person either returned $20 or $0. The probabilities of positive returns were either 80%, 50%, or 20%, and probabilities across the mock people changed every 30 trials, for a total of 90 trials. The neutral task was structured identically, except participants selected between three houses with varying probabilities of being open (returning $20) or locked (no return on investment). Participants were told their study compensation would be proportional to their performance on the task. The decision-phase of the task presented the response options to participants and their current amount of winnings, and was displayed until participants made a button press. The interval/anticipation phase consisted of the chosen option then being indicted by a surrounding colored box for 1s, followed by a jittered fixation cross for 1.5-3s. The outcome phase then displayed the outcome of the trial for 2s, followed by a jittered fixation cross for 1.5-3s. No participants needed to be removed from analyses due to poor performance (i.e., less than chance performance).

Facial Emotion Processing Task

The emotion processing task used here was identical to that used in prior research (1–3). Participants made button presses indicating decisions related to the sex of the poser while viewing human faces taken from the NimStim facial stimuli set. The faces contained either neutral or fearful expressions, presented either overtly or covertly, in alternating blocks. There

were an equal number of female and male faces. Overt faces were presented for 500 ms, with a 1200 ms inter-stimulus-interval displaying a blank screen with a fixation cross, in blocks of 8 presentations for a total block length of ~17 s. Covert face blocks used a similar design but were presented for 33 ms followed immediately by a neutral facial expression mask for 166 ms from the same actor depicted in the covert image, and the ISI was 1500 ms. Rest blocks that displayed a blank screen with a fixation cross and lasted 10 s were additionally included. The task was presented in two runs, each lasting ~8 min, during which each block type was presented 5 times. There were 10 total blocks for each stimulus category.

MRI Acquisition and Image Preprocessing

At the Arkansas site, fMRI data were acquired on a Philips Achieva 3T X-series scanner using a 32-channel headcoil. T1-weighted anatomic images were acquired with a MP-RAGE sequence (matrix = 192 × 192, 160 sagittal slices, TR/TE/FA = 7.5/3.7/9°, FOV = 256, 256, 160, final resolution = 1 × 1 × 1 mm resolution). Echo planar imaging sequences were used to collect the functional images using the following sequence parameters: TR/TE/FA = 2000 ms/30 ms/90°, FOV = 240 × 240 mm, matrix = 80 × 80, 37 axial slices (parallel to AC–PC plane to minimize OFC signal artifact), slice thickness = 2.5mm, and final resolution of 3 × 3 × 3 mm.

At the UW-Madison site, fMRI data were acquired on a GE MR750 3T scanner using an 8-channel headcoil. T1-weighted anatomic images were acquired with a MP-RAGE sequence (matrix = 256x256, 156 axial slices, TR/TE/FA = 8.2ms/3.2ms/12°, FOV = 25.6cm, final resolution = 1x1x1mm). EPI sequences used to collect the functional images used the following parameters: TR/TE/FA = 2000ms/ 25 ms/ 60, FOV = 24cm, matrix = 64 x 64, 40 sagittal slices, slice thickness = 4mm, original resolution was 4 x 3.75 x 3.75, and images were resampled to match the resolution of the UAMS data of 3x3x3mm.

Image preprocessing followed standard steps and was completed using AFNI software. In the following order, images underwent despiking, slice timing correction, deobliquing, motion

correction using rigid body alignment, alignment to participant's normalized anatomical images, spatial smoothing using a 8 mm FWHM Gaussian filter (AFNIs 3dBlurToFWHM that estimates the amount of smoothing to add to each dataset to result in the desired level of final smoothing), detrending, low frequency (128 s) bandpass filtering, and rescaling into percent signal change. Images were normalized using the MNI 152 template brain. Following recent recommendations (4, 5), we corrected for head motion related signal artifacts by using motion regressors derived from Volterra expansion, consisting of [R R^2 R_{t-1} R^2_{t-1}], where R refers to each of the 6 motion parameters, and separate regressors for mean signal in the CSF and WM. This step was implemented directly after motion correction and normalization of the EPI images in the image preprocessing stream. Additionally, we censored TRs from the first-level GLMs based on threshold of framewise displacement (FD) > 0.4. FD refers to the sum of the absolute value of temporal differences across the 6 motion parameters; thus, a cut-off of 0.4 results in censoring TRs where the participant moved, in total across the 6 parameters, more than ~0.4 mm plus the immediately following TR (to account for delayed effects of motion artifact). Additionally, we censored isolated TRs where the preceding and following TRs were censored, and we censored entire runs if more than 50% of TRs within that run were censored. This led to the removal of 1 participant. There were no differences between assault groups in head motion, $t(100)=-1.36$, $p=.18$.

Reinforcement Learning Model Fitting

We modeled participant behavior during the RL tasks using a modified version of the Rescorla-Wagner (RW) reinforcement learning model (6, 7). This model takes the form of $V_{t+1}=V_t+ \delta * \alpha$, where V refers to expected value of a chosen action, δ is a prediction error ($outcome_t - V_t$), and α is a learning rate that ranges from 0-1. The expected value of a chosen action changes from trial to trial based upon δ, such that a positive δ (i.e., receiving more than expected) increases expected value and a negative δ (i.e., receiving less than expected)

decreases expected value. The learning rate, α, controls the speed with which value expectations are updated, with higher learning rates leading to faster changes in expected value. We used a softmax function to transform value expectation into action probabilities through use of an exploration / exploitation parameter. Consistent with prior research (8), we tested four different RW-based models that manipulated whether the model was risk-sensitive (i.e., used a separate learning rate for positive and negative prediction errors) and whether the model updated the expected value of the unchosen option (i.e., anticorrelated updating of value expectation) in a factorial design. One cell therefore was the basic RW model (described above) using a single alpha to update value expectations with prediction errors. Anticorrelated models updated the value expectation of the unchosen options in the opposite direction of the prediction error (9, 10). For example, if the house on the right was found to be unlocked in the previous trial, value expectations for the left house being unlocked were reduced and vice versa. Risk sensitive models (8, 11) used a separate learning rate for positive and negative prediction errors. The anticorrelated and risk sensitive model updated the value of the unchosen option using the learning rate based on the sign of the prediction error.

The respective model's free parameters were fit by maximizing the sum of the log likelihood of action probabilities. We searched through continuous parameter space, rather than discretizing the parameters, using MATLAB's fmincon function, in which we constrained the searched parameter space for learning rates between 0-1 and for exploration/exploitation parameters between 0 and 15. We selected between different models, which had different numbers of free parameters, through likelihood ratio tests and calculating Akaike Information Criterion (AIC) correction on the sum of the log likelihoods. The value expectations and prediction errors of the best fitting model for each participant were carried forward to the fMRI analyses.

Ruling out the competing explanations of outcome versus prediction error processing. Given that reward outcomes are highly collinear with signed PEs in fMRI designs (12) (i.e., positive

PEs only occur on win trials; negative PEs only occur on loss trials), we used a model comparison approach to demonstrate that salience network activity better reflects PE encoding rather than reward outcome processing (12). In this approach, we fit a separate model to all participant's data in which the signed PE regressor was replaced with an outcome regressor indicating the direction of the outcome (1 = win; -1 = loss). We then compared the group-level distributions of β coefficients of salience network activity and adjusted R^2 values of model fit between the signed PE model and outcome model. This comparison demonstrated that β coefficients of salience network activity to signed PEs was significantly larger than for outcomes, $t(210)=3.58$, $p<.001$, and that adjusted R^2 values were significantly higher for the signed PE model versus the outcome only model, $t(210)=2.34$, $p = .02$. These analyses demonstrate that SN encoding best reflects the signed magnitude of the prediction error, rather than simple outcome processing.

Ruling out confounds related to medication usage and scanning site. When the primary models were repeated including an additional covariate for psychotropic medication usage, all reported results above remained essentially identical: assault exposure severity associations with SN encoding of negative prediction errors, $t(98)=-3.29$, $p=.001$ and the group x facial expression x duration interaction in the FEP task, $t(211)=2.57$, $p=.011$ remained. Though all models used site as a covariate, when also separating the groups by site, the opposing salience network responses to negative PEs and facial emotion processing as a function of assault and CTQ scores were retained (Supplemental Figure S3A and S3B), demonstrating the overall effects are not an artifact of combining data across sites.

Supplemental Figures

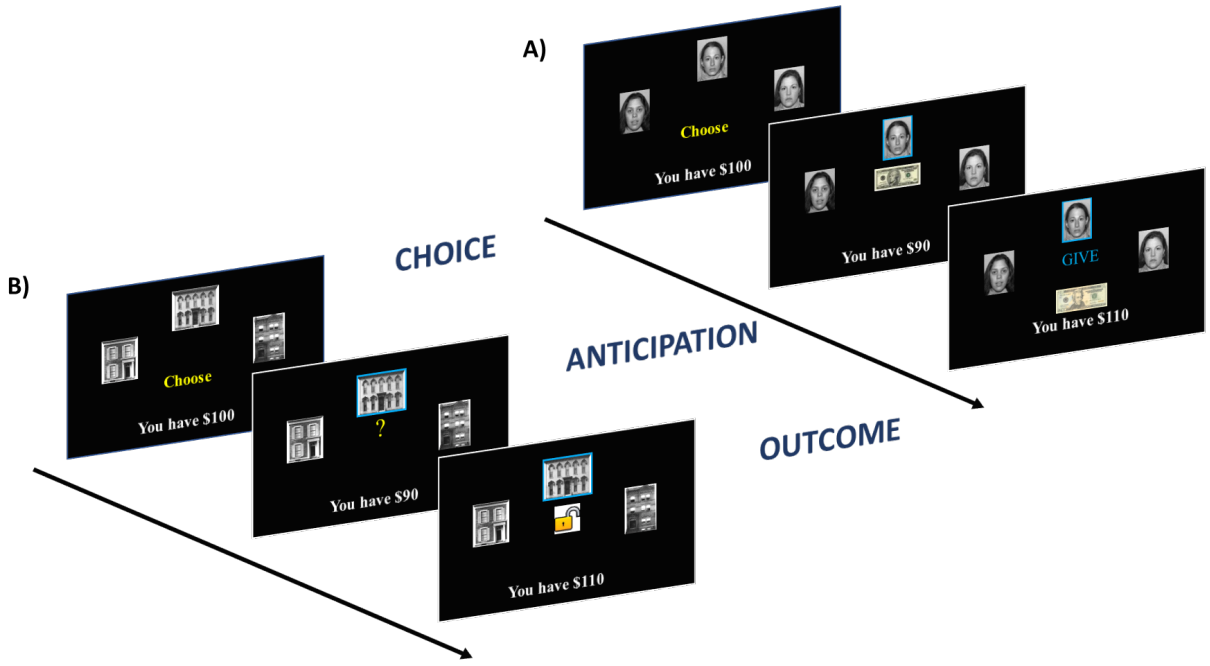

Supplemental Figure S1. Depiction of the three-arm bandit tasks using social (A) or neutral (i.e., non-social) (B) stimuli. Participants selected one of the three response options to earn points. The three options were associated with probabilities of reward of 80%, 50%, or 20%, and the probability associated with each arm changed every 30 trials. The choice phase continued until participants made a response. The chosen option was then highlighted with a colored box for 1s and then followed by the jittered interval/anticipation phase, which lasted for 1.5-3s. The outcome phase then presented the outcome of the trial for 2s followed by a jittered fixation cross for 1.5-3s.

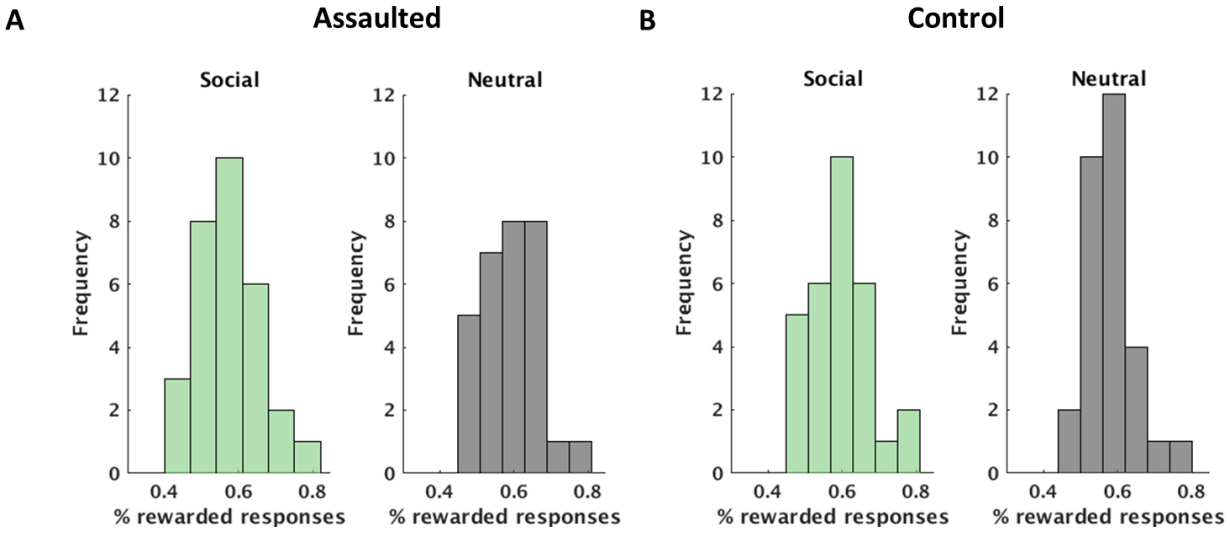

Supplemental Figure S2. Histograms of task performance for both the social and non-social RL task for the assaulted (A) and control (B) participants. Task performance is defined as the proportion of reward trials. Random chance performance would be .33; thus, all participants performed above chance levels of performance.

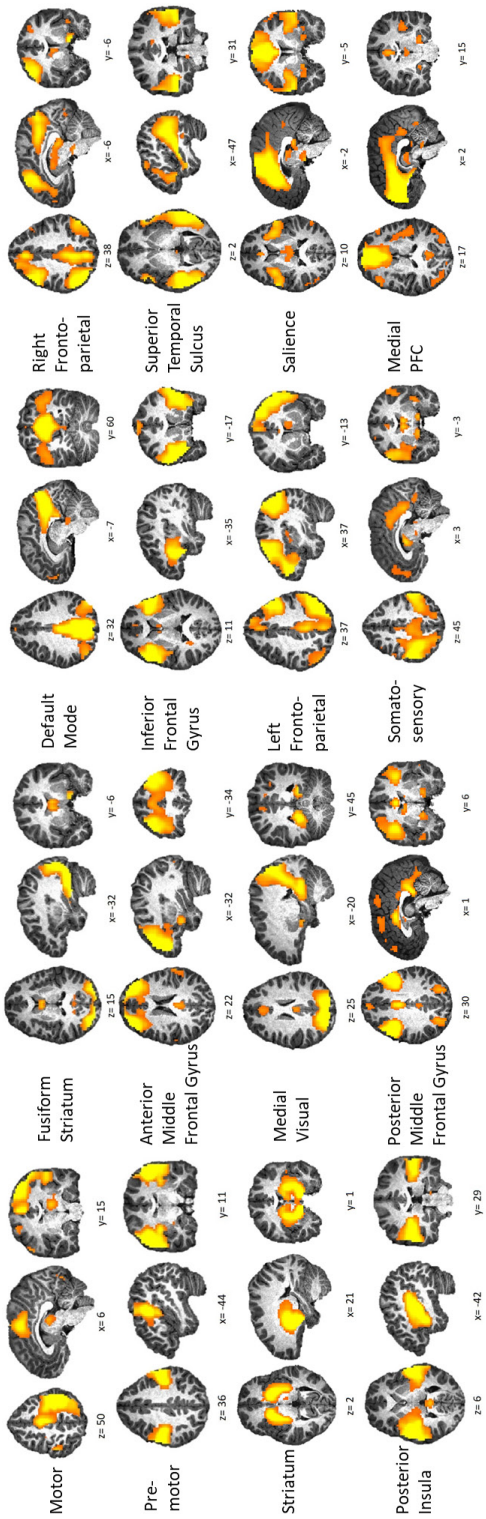

Supplemental Figure S3. Graphical depiction of each of the functional networks identified with ICA.

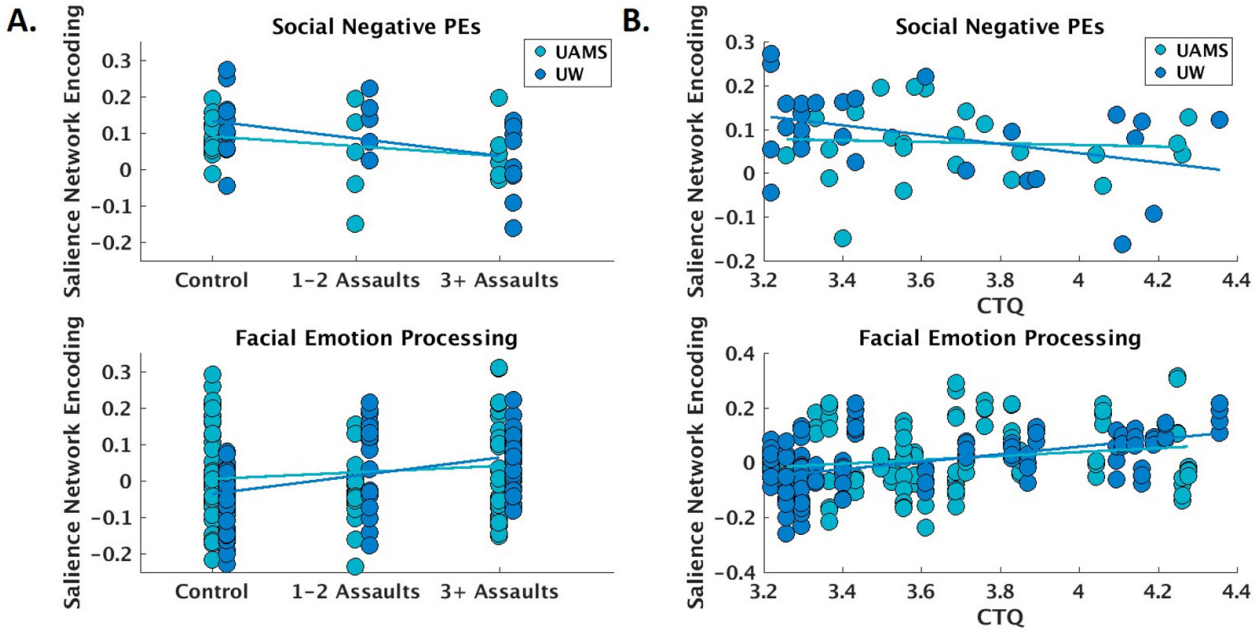

Supplemental Figure S4. Depiction of relationship between assault exposure (A) and Childhood Trauma Questionnaire (CTQ) (B) and salience network (SN) encoding of negative prediction errors during social RL (where group-level effects were most robust) and facial emotion processing as a function of scanning site. UW = University of Wisconsin; UAMS = University of Arkansas for Medical Sciences.

Supplemental References

1. Bryant RA, Kemp AH, Felmingham KL, Liddell B, Olivieri G, Peduto A, *et al.* (2008): Enhanced amygdala and medial prefrontal activation during nonconscious processing of fear in posttraumatic stress disorder: An fMRI study. *Hum Brain Mapp*. 29: 517–523.

2. Rauch SL, Whalen PJ, Shin LM, McInerney SC, Macklin ML, Lasko NB, *et al.* (2000): Exaggerated amygdala response to masked facial stimuli in posttraumatic stress disorder: a functional MRI study. *Biol Psychiatry*. 47: 769–776.

3. Williams LM, Liddell BJ, Kemp AH, Bryant RA, Meares RA, Peduto AS, Gordon E (2006): Amygdala–prefrontal dissociation of subliminal and supraliminal fear. *Hum Brain Mapp*. 27: 652–661.

4. Power JD, Mitra A, Laumann TO, Snyder AZ, Schlaggar BL, Petersen SE (2014): Methods to detect, characterize, and remove motion artifact in resting state fMRI. *Neuroimage*. 84: 320–341.

5. Siegel JS, Power JD, Dubis JW, Vogel AC, Church JA, Schlaggar BL, Petersen SE (2014): Statistical improvements in functional magnetic resonance imaging analyses produced by censoring high-motion data points. *Hum Brain Mapp*. 35: 1981–1996.

6. Rushworth MFS, Behrens TEJ (2008): Choice, uncertainty and value in prefrontal and cingulate cortex. *Nat Neurosci*. 11: 389–397.

7. Sutton RS, Barto AG (1998): *Learning: An Introduction*. Cambridge, MA: MIT Press.

8. Hauser TU, Iannaccone R, Walitza S, Brandeis D, Brem S (2015): Cognitive flexibility in adolescence: Neural and behavioral mechanisms of reward prediction error processing in adaptive decision making during development. *NeuroImage*. 104: 347–354.

9. Gläscher J, Daw N, Dayan P, O'Doherty JP (2010): States versus Rewards: Dissociable Neural Prediction Error Signals Underlying Model-Based and Model-Free Reinforcement Learning. *Neuron*. 66: 585–595.

10. Hauser TU, Iannaccone R, Ball J, Mathys C, Brandeis D, Walitza S, Brem S (2014): Role of the Medial Prefrontal Cortex in Impaired Decision Making in Juvenile Attention-Deficit/Hyperactivity Disorder. *JAMA Psychiatry*. 71: 1165–1173.

11. Niv Y, Edlund JA, Dayan P, O'Doherty JP (2012): Neural Prediction Errors Reveal a Risk-Sensitive Reinforcement-Learning Process in the Human Brain. *J Neurosci*. 32: 551–562.

12. Erdeniz B, Rohe T, Done J, Seidler R (2013): A simple solution for model comparison in bold imaging: the special case of reward prediction error and reward outcomes. *Front Neurosci*. 7. doi: 10.3389/fnins.2013.00116.